Geomechanical modelling of the Steinernase landslide (Switzerland)

L. Laloui, A. Ferrari & Ch. Bonnard[(*)]

Soil Mechanics Laboratory (LMS), Ecole Polytechnique Fédérale de Lausanne (EPFL), Switzerland.

[(*)]*Presently independent consultant, PBBG SA, Lausanne.*

ABSTRACT: A geomechanical model was developed to analyse the behaviour of a natural slope located on the bank of the Rhine River between the towns of Stein and Mumpf in Switzerland. The slope is affected by a landslide and three strategic infrastructure assets are located at its toe. An intense monitoring campaign made it possible to identify pore water pressure evolution as the main cause for movement accelerations and to detect the presence of a multiple slip surface system. Advanced coupled finite element hydrogeological and geomechanical models have been used to analyse the landslide behaviour. After being calibrated and validated, the model was applied to improve the understanding of the physical processes involved and to predict the slope behaviour under different scenarios.

1 INTRODUCTION

The Steinernase landslide affects a natural slope on the bank of the river Rhine between the towns of Stein and Mumpf in the canton of Aargau (Switzerland) (Figure 1). Slowly-moving slides of limited size are quite frequent in these mountainous or hilly areas and do not represent a major challenge for land planning, unless they may display occasional crises, generally due to exceptional climatic conditions. Such a situation is even more critical if major infrastructure assets cross the slide area; under the effect of an acceleration phase of the slide, these works may be affected or even blocked, which represents a potential serious hazard that cannot be analysed in terms of probability analysis, as the number of recorded past events is generally very small. This special situation occurs in the present case study since three infrastructure assets are located at the slope toe, namely a railway, a highway and a cantonal road connecting Zurich and Basel.

The presence of this slide had been known for many years. Due to the strategic importance of the potentially involved infrastructure, a monitoring campaign was started in 1986 to assess the dangers posed by the landslide, but it was difficult for the authorities to determine if the slide might be liable to experience a serious crisis, in which conditions (maybe related to climate change), and what would be the consecutive displacements. A simple limit equilibrium model is unable to answer to such questions and only a detailed hydro-geological and geomechanical approach, implying the development of finite element models, allows an appropriate answer so such questions.

In this sense, an extensive study was recently started in which geological, hydrological and geotechnical aspects were addressed (EPFL, 2008). Advanced finite element hydrogeological and geomechanical models were set up using a methodology that was already developed a few years ago for the La Frasse landslide in Switzerland (Tacher et al., 2005). The La Frasse landslide was much larger than the Steinernase case study and displayed major crisis episodes in its lower part with displacements of nearly 4 m in a few months. The major challenge in this present case, extending over an area of some 7 ha only and affected by minor crises of 1 to 2 cm in winter, was to know beforehand if an appropriate model would be precise enough to reproduce the displacements observed during crisis episodes. Once calibrated and validated the model could be used to allow the quantification of expected displacements in modified conditions, like different rainfall conditions or the construction of a drainage scheme aiming at protecting the main highway and the main railway line between Basel and Zurich.

The first required condition to solve this problem was to precisely describe the geological conditions and to include the various observed slip surfaces in the model, as well as to take the unsaturated conditions into account, which determine the absence of significant movements during most of the year, so as to reproduce the proper mechanism of this slide.
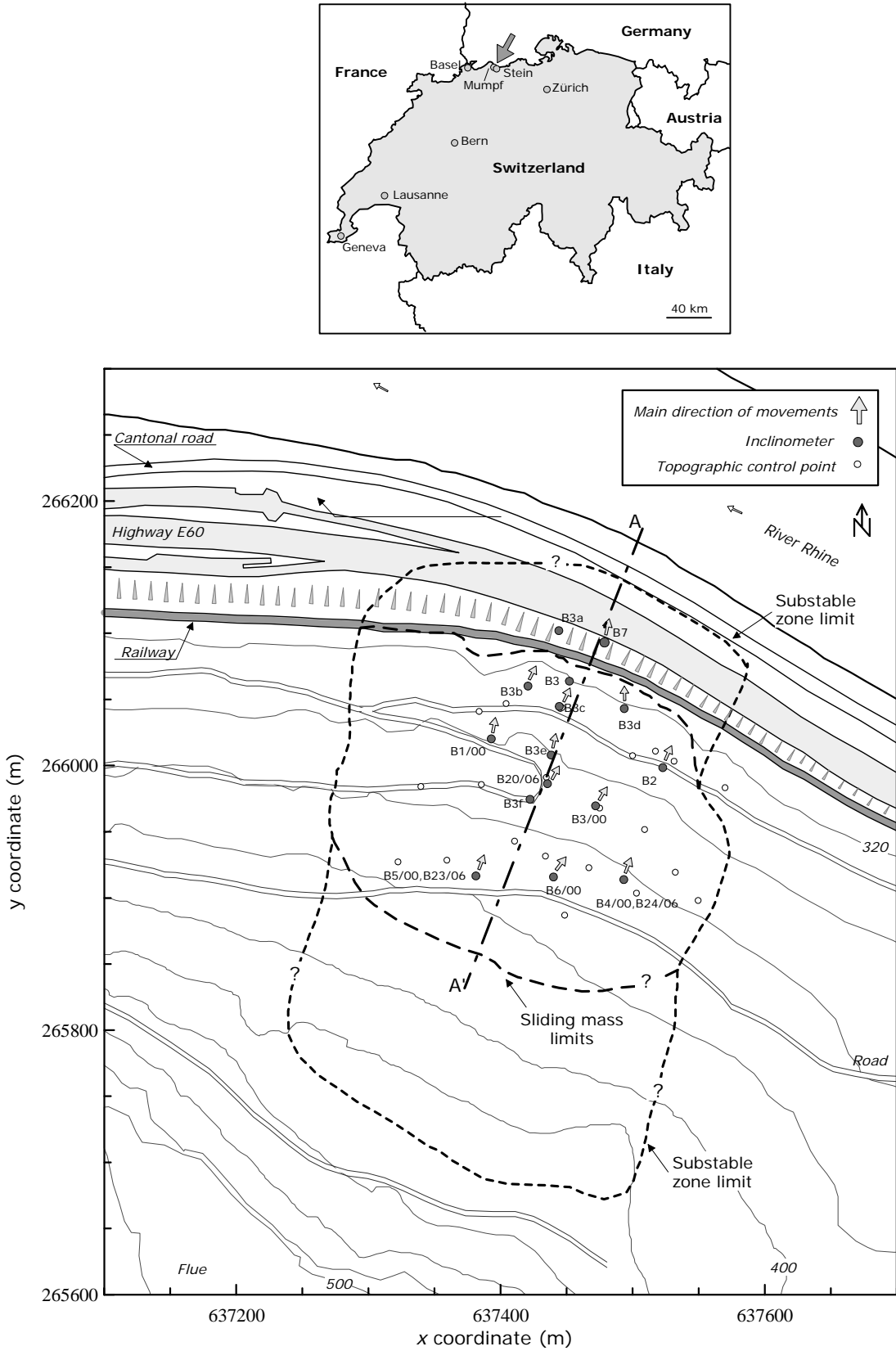
Figure 1. Location and general plan of the landslide showing the position of inclinometers and topographic control points. Limits of the active and substable zones and main direction of movements are shown. (Coordinates according to the Swiss reference system).

2 DESCRIPTION OF THE LANDSLIDE

2.1 *Geological setting*

The Steinernase landslide is situated in the Jura hills of Switzerland at the edge of the German Black Forest crystalline outcrop. From this location results a quite variable rock series with Permian siltstones at the base of the slope near the Rhine River. The siltstones are superposed by Triassic sandstones on which rest Triassic evaporites. The series is terminated at the top by Jurassic limestones. The sliding mass itself is composed of quaternary sediments, mostly formed of colluvial clays with some alluvial sediments from the Rhine River at the toe of the slope. The failure mechanism is located in the slope clay, close to the bedrock.

2.2 *Morphology*

A systematic monitoring of the landslide started in 1986, when two inclinometers - still in use - were installed at the slope toe in proximity to the railway and roads. Inclinometer B7, located between the railway and the highway, has shown downhill movements with a fairly continuous rate of about 1.5 mm per year. On the other hand, inclinometer B3, positioned close to the railway, has indicated the existence of a well-defined slip surface and the occurrence of episodic accelerations in some winter periods. Although the movement rates were not alarming, an extensive measurement campaign, started in 1995 and still under way, was undertaken to comprehensively assess the potential dangers to the infrastructure, during which inclinometers, piezometers and topographic control points were installed. The information collected over the last 13 years made it possible to assess the active zone, approximately 300 m width and 230 m length (Geotest, 2006), which is reported in Figure 1. Evidence of superficial instabilities led to the conclusion that this active zone is part of a wider substable zone which extends longitudinally from the beginning of the slope main scarp to the cantonal road.

2.3 *Kinematical features*

Readings pointed out that the displacements are directed towards the slope fall line (Figure 1). Moreover, inclinometer profiles clearly show the presence of a multiple surface failure mechanism. As an example, data on displacements over time from inclinometer B3c for two different depths are plotted in Figure 2. The plot indicates that during crisis episodes, the more superficial part of the landslide body undergoes noticeable relative movements with respect to the deeper part and a relative displacement accumulates.

Pore water pressure variation within the slope was recognized as the main cause for accelerations. The trend of total head recorded at 10 m depth is also plotted in Figure 2 for borehole B3c. Inclinometer reading delays do not allow to assess the exact instants in which movements start and end; however it is worthwhile to note that displacement sudden increases coincided with total head peaks.
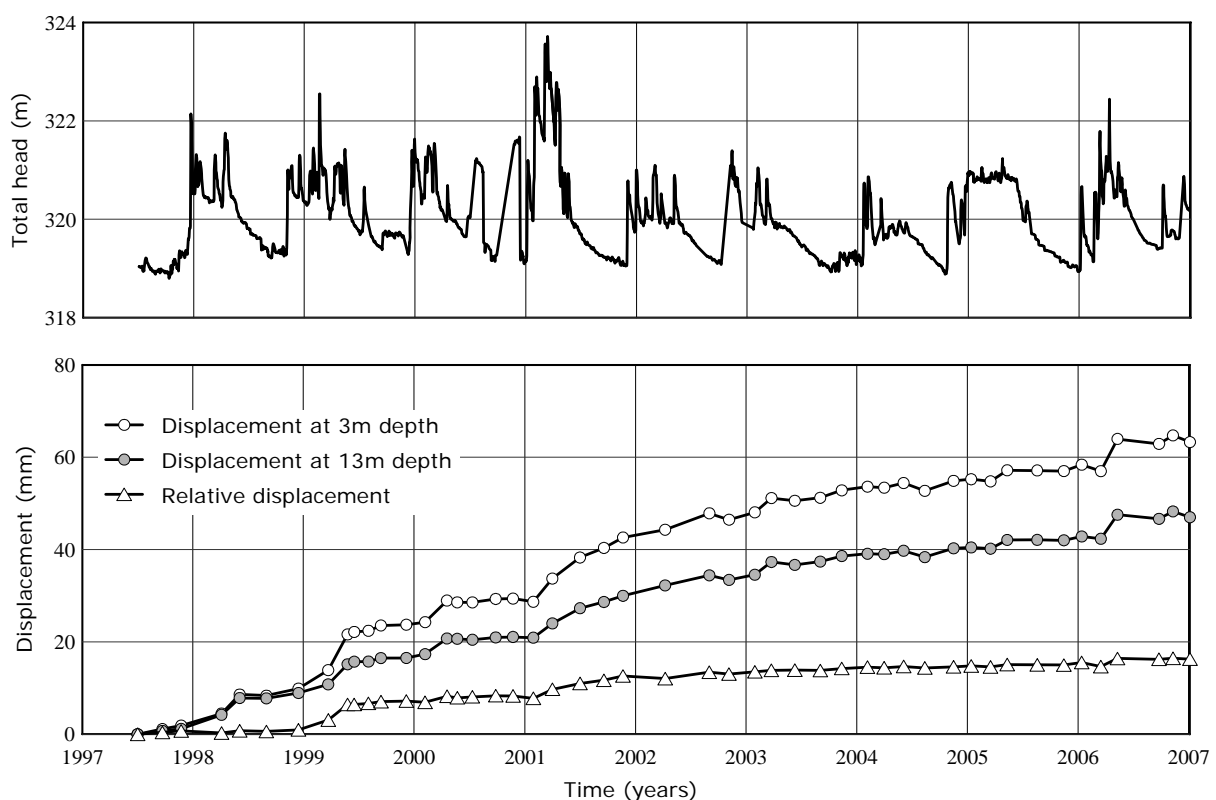

Figure 2. Total head at 10m depth and displacements at two different depths registered at the borehole B3c.
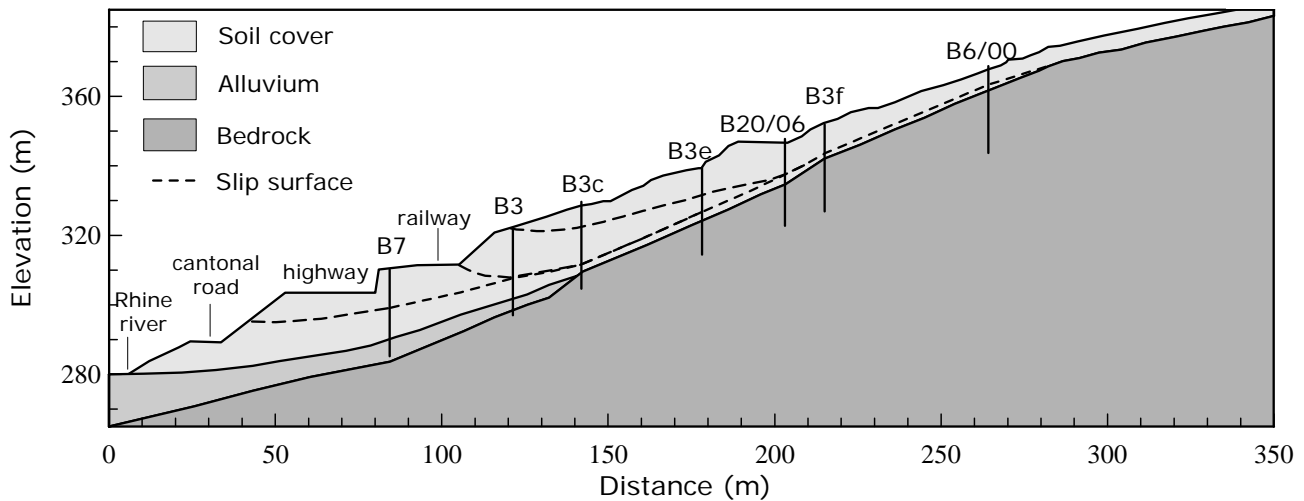
Figure 3. Cross section along the centre of the landslide, indicating the multiple slip surface system as interpreted from inclinometer readings.

2.4 *The multi-surface failure mechanism*

A schematic of the multiple-surface system is depicted in Figure 3, in which a cross section along the centre of the active zone is reported (profile A-A' in Figure 1). A detailed position of the slip surface at the slope toe cannot be identified, since no displacement measurement has been performed in that zone. However, the general trend of the slip surfaces suggested that the deep-seated sliding surface reaches the slope between the cantonal road and the highway. In this sense, dangers for the infrastructures would be most related to a possible reactivation of deep movements.

2.5 *Involved materials*

Boreholes data pointed out the presence of three main materials in the slope (Figure 3): (i) the soil cover (ii) the bedrock and (iii) the Rhine Alluvium.

The multiple surface failure mechanism develops entirely within the soil cover. In spite of some heterogeneity in index properties at a local scale, soil of the landslide body is homogenous at the scale of the slope. As an example, the grain size distribution is depicted in Figure 4 for samples coming from different boreholes and depths; a certain homogeneity can be observed.

No experimental evidence was available for the retention properties of the soil layer. As discussed later in the text, the transition from the fully to the partially saturation state is considered an important aspect for the occurrence of displacements. The model proposed by Arya and Paris (1981) was used, allowing information on the retention behaviour of the soil based on the knowledge of its grain size distribution and density. An averaged grain size distribution was used, based on the ones presented in Figure 4.
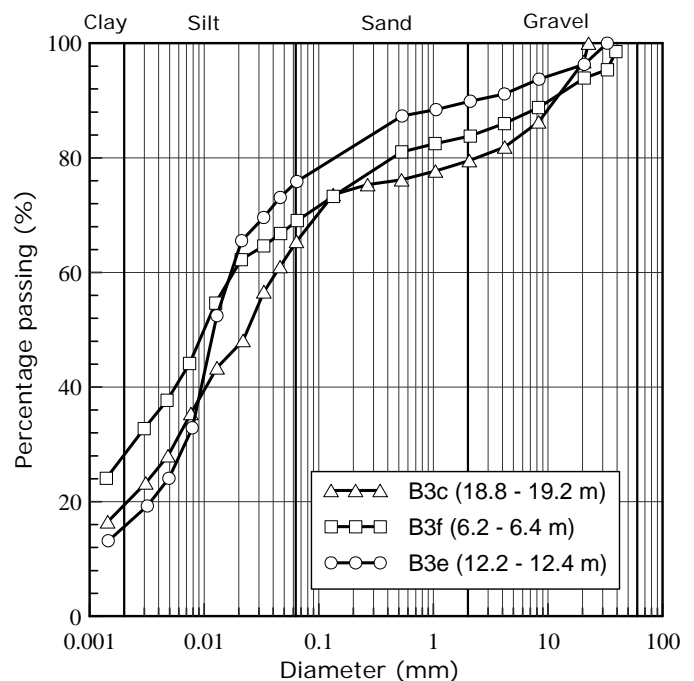

Figure 4. Grain size distribution of samples obtained from different boreholes at different depths (after Geotest, 1997).

The obtained retention curve presented an air entry value (value of suction at which the soil starts to dry) in the order of 10-20 kPa. This value is in accordance with the presence of the sand and gravel fractions in the grain size distributions.

Shearing resistance parameters were obtained by direct shear tests, performed on specimens collected on the slip surfaces. Obtained values, with some scatter, were in the range 24° – 27° for the shearing resistance angle, while the cohesion was negligible. Test results provided slightly lower values of the shearing resistance angle for the most superficial slip surface.

3 THE FINITE ELEMENT MODELLING

The analysis of the data obtained from the instrumented boreholes showed that accelerations are observed when total head peaks take place. Moreover, the groundwater table does not seem to reach the topographic surface, even during the more intense pore water pressure raising; during these crisis episodes the free surface seems to reach the level of the most superficial slip surface.

These considerations led to the conclusion that a coupled hydro-mechanical approach was a proper solution to analyse the landslide behaviour with the aim to relate pore water pressure variations and movements in a quantitative way. In particular the partial saturation of the soil and the transition from the partially to the fully saturated state must be explicitly taken into account, especially considering that the activation of the most superficial slip surface could depend on a reduction of the suction acting on it.

An extensive analysis of the hydrogeological features of the slope was firstly performed by the Laboratory of Engineering and Environmental Geology (GEOLEP) at the EPFL (EPFL, 2008). This study pointed out the role of several key factors on the evolution of pore water pressure within the slope, such as infiltration, preferential flows and vegetation. A 3D finite element hydrological model was calibrated and validated in order to predict the pore water pressure evolution in the area of interest for the years 2000, 2001 and 2006. The outcome of the hydrogeological model was used as input for the geomechanical model by means of a coupling between the two models, in a similar manner to that used by François et al. (2007). The general outline of the coupling between the hydrogeological model and the geomechanical model is presented in Figure 5. Pore water pressure variations over time and space, obtained from the hydrogeological model for the considered years, were imposed as boundary conditions at the nodes of the geomechanical model.

In the general formulation of the coupling, computed strains in the geomechanical model can be used to update parameter values of the hydrogeological modelling with time, such as the permeability and the air entry value of the involved materials. In the present case, due to the limited values of displacements which were observed, this part of the coupling was neglected.

3.1 *Formulation of the hydro-geomechanical coupling*

In the formulation of the model, the three-phase medium (solid, water, air) is considered as an equivalent two-phase medium with a compressible liquid phase (it is assumed that air bubbles are trapped within water). The interaction between the pore fluid pressure and the mechanical behaviour of the solid skeleton is obtained with a Biot-type mathematical formulation (Biot, 1956), in which the mass and momentum of the fluid and solid phases are conserved. A thermodynamic description of the general form of the field equations is given in Laloui et al. (2003). The mass conservation equation of the soil is described by:

$$n\left(\beta_f S_r + \frac{dS_r}{dp}\right)\partial_t p + div \ \partial_t \mathbf{u}_{rf} + S_r \ div \ \partial_t \mathbf{u}_s \ = \ 0 \ (1)$$

where p is the pore fluid pressure (compression pressure taken as positive), β_f is the compressibility of water, S_r is the degree of saturation and n is the porosity. In this formulation, the solid grains are treated as incompressible while the skeleton compressibility is expressed by the constitutive law. The velocity vector of the fluid infiltration $\partial_t \mathbf{u}_{rf}$ links the absolute velocities of the fluid, $\partial_t \mathbf{u}_f$, and of the solid skeleton, $\partial_t \mathbf{u}_s$, by:

$$\partial_t \mathbf{u}_{rf} \ = \ n\left(\partial_t \mathbf{u}_f - \partial_t \mathbf{u}_s\right) \tag{2}$$

Darcy's law is then introduced to link the infiltration velocity with the hydraulic head:

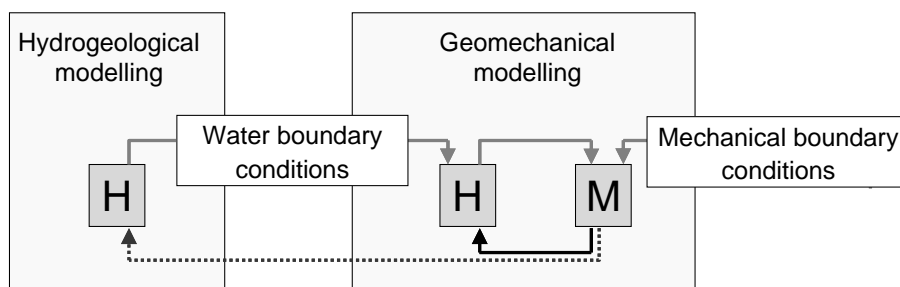$$\partial_t \mathbf{u}_{rf} = -\mathbf{K}^* \ \mathbf{grad}\left(p + \rho_f \mathbf{gx}\right) \tag{3}$$

Figure 5. Outline of the coupling between the hydrogeological and the geomechanical modelling.

where ρ_f is the volumetric mass of the fluid (water), $\mathbf{g}$ is the vector of gravity acceleration, $\mathbf{x}$ is the position vector and $\mathbf{K}^*$ is the tensor of the kinematic soil permeability. In unsaturated soils, $\mathbf{K}^*$ is a function of the degree of saturation S_r and is obtained by the multiplication of the tensor of the saturated permeability $\mathbf{K}$ by a scalar function, $k_r(S_r)$:

$$\mathbf{K}^* = k_r \, \mathbf{K} \tag{4}$$

The expression proposed by van Genuchten (1980) was used:

$$k_r = \left(\frac{S_r - S_{r,res}}{1 - S_{r,res}} \right)^3 \tag{5}$$

where $S_{r,res}$ is the residual degree of saturation. Retention curves relate the degree of saturation to the pore fluid pressure. The following expression is used (van Genuchten, 1980):

$$\begin{cases} S_r = S_{r,res} + \dfrac{1 - S_{r,res}}{\left[1 + \left(\alpha \dfrac{p}{\rho_f g} \right)^2 \right]^{1/2}} & \text{if } p < 0 \\[4mm] S_r = 1 & \text{if } p \geq 0 \end{cases} \tag{6}$$

where α is a material parameter. As a first approximation, hysteretical effects and retention behaviour dependency on density are neglected by assuming a constant value for α. Thus, the mass conservation is expressed by:

$$S_r \, div \, \partial_t \mathbf{u}_s = div \left[\mathbf{K}^* \, \mathbf{grad} \left(p + \rho_f \mathbf{gx} \right) \right] + $$
$$-n \left(\beta_f S_r + \frac{dS_r}{dp} \right) \partial_t p \tag{7}$$

As it can be seen, the temporal variation of the solid displacement (left side term) may be modified by the Darcy's flow (first right side term) and/or by the pore fluid pressure variation (second right term).

The soil equilibrium equation is given by:

$$\mathbf{DIV} \, \boldsymbol{\sigma} - \rho \mathbf{g} = \mathbf{0} \tag{8}$$

where $\boldsymbol{\sigma}$ is the total (Cauchy) stress tensor with compression stresses taken as positive, and ρ is the total average mass density $\rho = \rho_d + n \, S_r \, \rho_f$, with ρ_d being the mass density of the solid skeleton. The behaviour of the solid matrix is assumed to be governed by the generalised Bishop's effective stress equation (Schrefler, 1984; Nuth & Laloui, 2008) given by:

$$\boldsymbol{\sigma}' = \boldsymbol{\sigma} - S_r p \boldsymbol{\delta} \tag{9}$$

with $\boldsymbol{\sigma}'$ being the effective stress tensor and $\boldsymbol{\delta}$ is Kroenecker's delta. Eq. (9) ensures a smooth transition from the partial to the full saturation condition, providing the Terzaghi effective stress definition when $S_r = 1$. The intensity of the measured displacement justifies the assumption of small strain approach. The effective stress tensor may be expressed in terms of the total strain tensor $\boldsymbol{\varepsilon}$ and the elasto-plastic constitutive tensor $\mathbf{C}$; thus the momentum conservation equation takes the form:

$$\mathbf{DIV} \left\{ \mathbf{C} : \boldsymbol{\varepsilon}(\mathbf{u}_s) \right\} = \rho \mathbf{g} - S_r \, \mathbf{grad} \, p \tag{10}$$

Equations (7) and (10) comprise the two field equations with two unknowns $(\mathbf{u}_s, p)$. These mathematical and constitutive formulations were applied using the software Z_SOIL®.

3.2 Features of the geomechanical model

Inclinometer profiles indicate that strains are concentrated along slip surfaces, while the rest of the landslide moves as a rigid body. Two soil constitutive laws were therefore adopted, namely a Modified Cam Clay elasto-plastic model (Roscoe and Burland, 1968) for the material at the slip surfaces and an elastic model with proper rigidity for the materials that are not expected to experience appreciable strains. Although unsaturated conditions are not explicitly taken into account in the constitutive laws, suction effects are considered through the definition of the effective stress (Eq. 9) and the variations of permeability (Eq. 5).

The positions of slip surfaces were carefully reconstructed from the inclinometer profiles at the instrumented boreholes. This information was used to build a 2D mesh for the geomechanical model. The mesh was created on a cross-section passing through the centre of the landslide (Figure 3). An unstructured mesh was selected, including 1694 nodes and 1554 isoparametric 4-node elements (Figure 6). Three independent slip surfaces were introduced to take the multiple surface failure mechanism into account, allowing a better reproduction of relative displacements among the various sliding surfaces. As to the boundary conditions, fixed nodes were assumed at the bottom of the domain for the deepest layers of alluvium and bedrock. Only horizontal displacements were prevented for the nodes of the left edge, corresponding to the Rhine River, while equivalent loading forces were applied at the right edge. A specific parametric study was performed, testing different lateral stress distributions on this edge, resulting in the assumption of an active state.
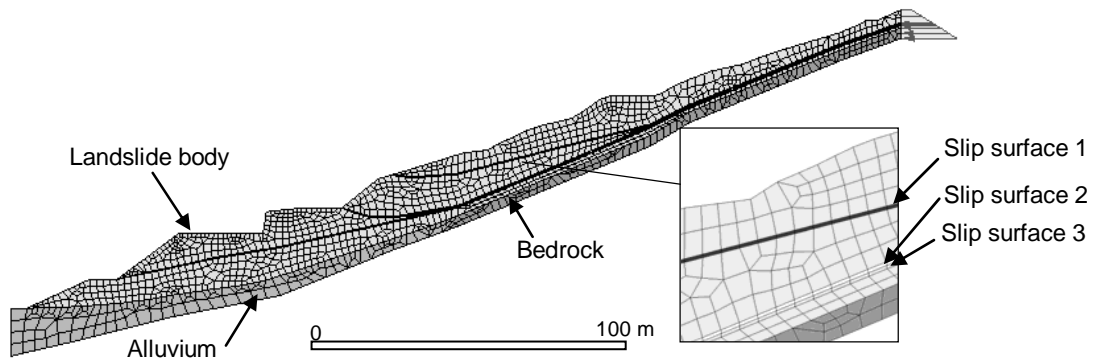
Figure 6. Finite element mesh for the geomechanical model.

The initial state of stress is the one induced by the soil weight at rest. The hydraulic boundary conditions were inherited from the hydrogeological model. A fixed total head of 280 m was assigned to the nodes at the left edge to take into account the Rhine River the level of which is controlled by a dam downstream of the landslide site. For the rest of the nodes, pore water pressure evolution at each time step was imposed, using the values obtained in the hydrogeological model.

4 NUMERICAL SIMULATIONS

The model was first calibrated for the period between 1 January, 2000 and 31 December, 2001, during which two accelerations were detected (Figure 2). For this reference period, pore water pressure distributions within the slope were obtained as a result of the hydrogeological model calibration. Ranges for material parameters were chosen taking the indications coming from laboratory tests results into account (Geotest, 1997). By comparing observed and computed displacements in several points of the slope during the calibration phase, the values for model parameters were refined. Table 1 shows the material parameters obtained for the slip surfaces.

As a result of the calibration, the model well reproduced the observed displacements through the entire domain for the considered period (Figure 7): larger displacements were correctly predicted for the upper part of the landslide body.

Table 1. Material parameters for the slip surfaces.

Parameter	Slip Surface		
	1	2	3
Slope of the virgin compression line	0.1	0.1	0.1
Slope of the swelling line	0.05	0.05	0.05
Poisson's ratio	0.3	0.3	0.3
Shearing resistance angle	23°	24°	25.5°

1/01/2000, day 0, reference date for displacement computation.

1/03/2000, day 60, accumulated horizontal displacements at the end of the first considered acceleration phase.

18/04/2001, day 473, accumulated horizontal displacements at the end of the second considered acceleration phase.

31/12/2001, day 730, accumulated horizontal displacements at the end of the 2 years considered in the calibration phase.

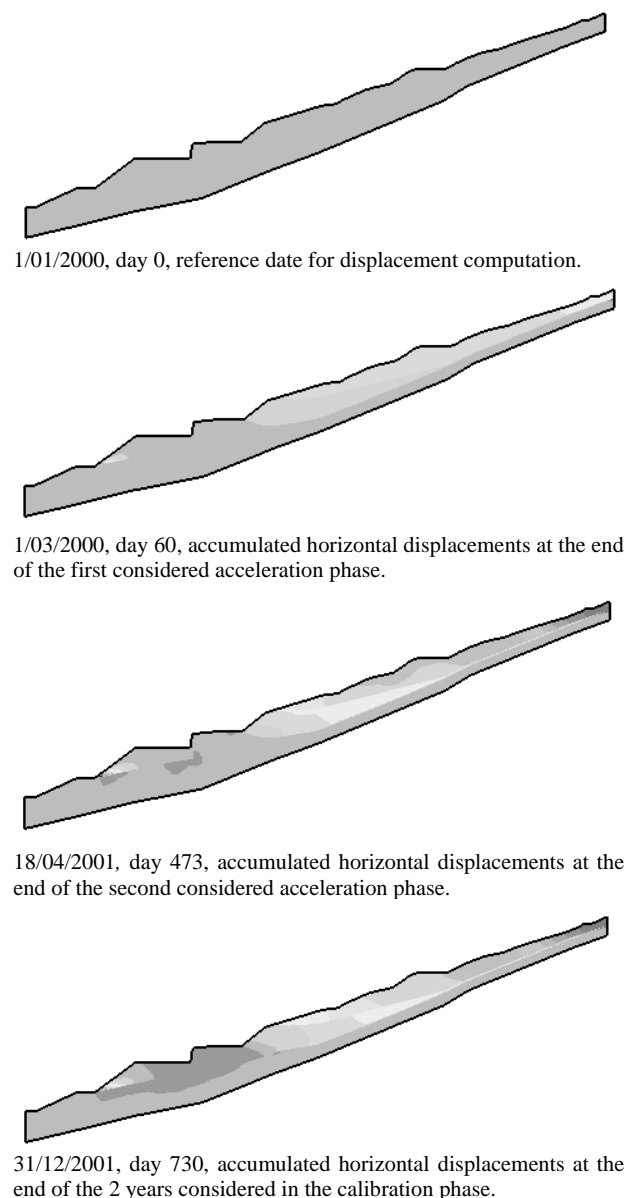|		
-7.000e-002	-4.300e-002	-1.600e-002
-6.550e-002	-3.850e-002	-1.150e-002
-6.100e-002	-3.400e-002	-7.000e-003
-5.650e-002	-2.950e-002	-2.500e-003
-5.200e-002	-2.500e-002	2.000e-003
-4.750e-002	-2.050e-002	6.500e-003

Figure 7. Computed horizontal displacement patterns at different times (negative sign refers to downhill displacements).
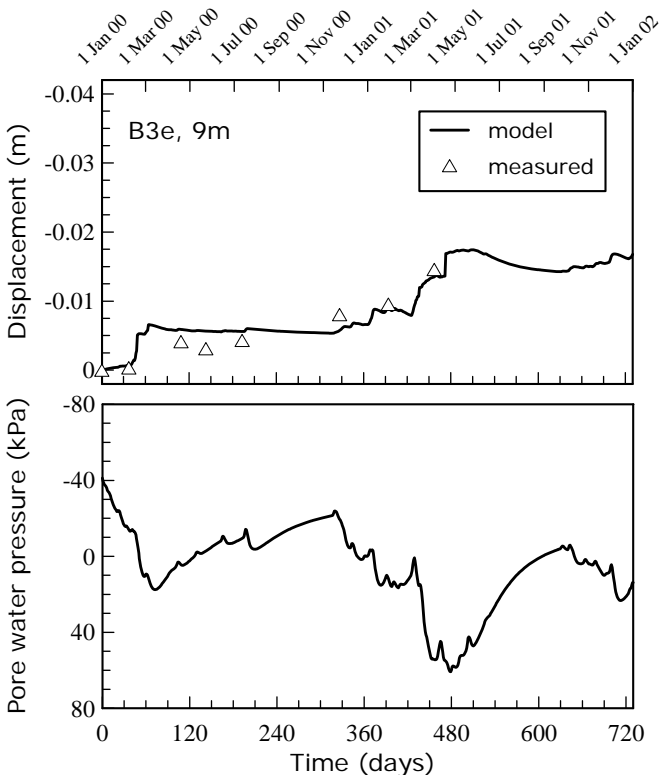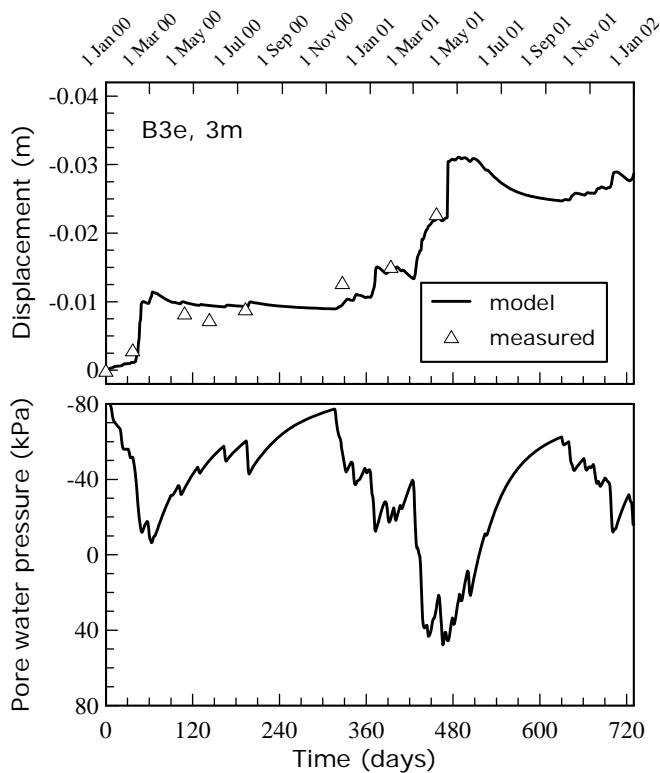
Figure 8. Computed and measured horizontal displacements and evolution of the computed pore water pressures at borehole B3e for the period 1/01/2000 – 31/12/2001 (negative sign refers to downhill displacements).

For a quantitative assessment of the model capabilities, Figure 8 shows observed and computed displacements for borehole B3e at two different depths, namely 3 and 9 m. The plot shows that accelerations that occurred during crisis periods are reproduced well, both in terms of durations and accumulated displacements. In accordance with measurements in the field, larger displacements are computed for the more superficial part of the slope. Higher displacement values with respect to the measured ones are predicted for the borehole B3e at 3m during the second acceleration phase. This result is in accordance with the fact that the installed inclinometer in that borehole was sheared during that event.

Computed pore water pressures for the same nodes are also represented in Figure 8 (positive values refer to compressions). The plots allow the appreciation of the quantitative correlation between the evolution of displacement and the evolution of pore water pressure, which constitutes the key point of the coupled hydro-geomechanical model. These plots also indicate that displacements in the more superficial part of the slope can be initiated by the transition from negative (suction) to positive values of pore water pressure.

Once calibrated, the model has been used in order to simulate the landslide behaviour when subjected to pore water pressure distributions induced by different rainfall patterns and to assess possible stabilization strategies.

In the first case, pore water pressure distributions for the period 2000-2001 provided by the hydro-geological model were incremented by 10% in order to simulate, as a first approximation, an increase in the total amount of rainfall, without a significant change in rainfall pattern. Horizontal displacements for the borehole B3e at 3m depth are reported in Figure 9. The comparison with the displacement in the same point associated to the original pore water pressure distribution indicates an almost linear increase of 10% in the final cumulated displacement. A constant and diffused increase (with small amplitude) of the pore water pressure distribution within the slope will not therefore significantly change the overall landslide response, affecting only the final cumulative displacement.
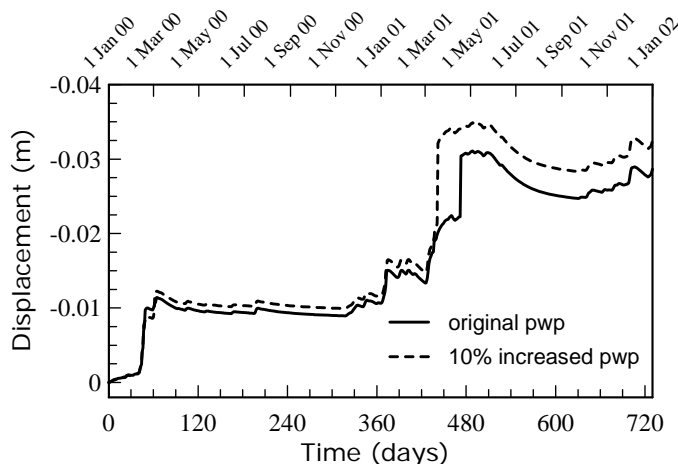

Figure 9. Predicted horizontal displacements for 10% pore water pressure (pwp) increase, at borehole B3e at 3m depth.
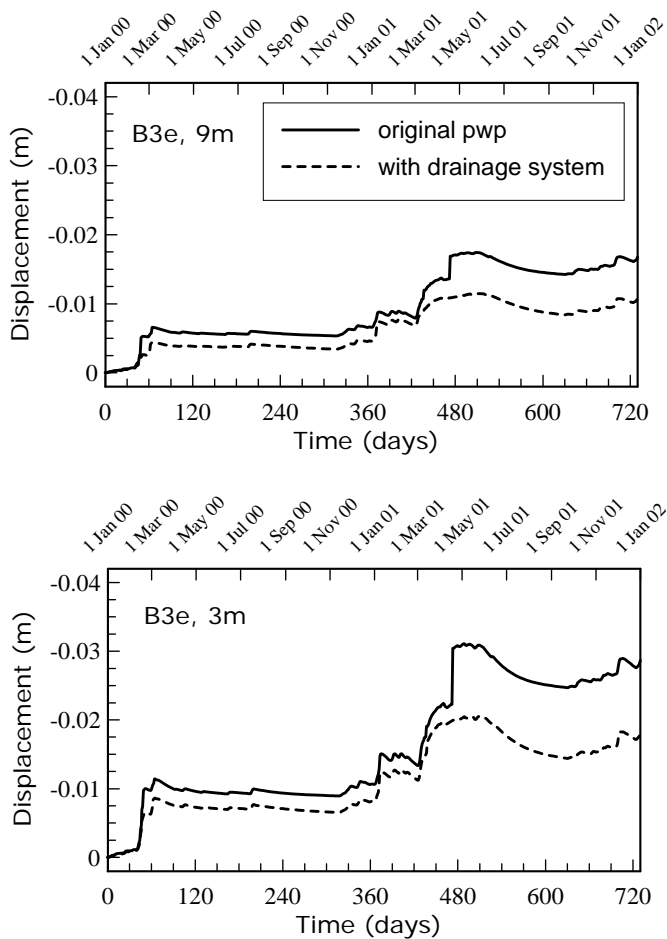
Figure 10. Predicted horizontal displacements at borehole B3e for the scenario with sub-horizontal drains.

As an example of the model application to assess stabilization strategy efficiency, displacement trends for the years 2000-2001 were predicted for the case in which a system of sub-horizontal drains at the slope toe was installed. This analysis considered 50 m long drains drilled from the cantonal road. The presence of the drains was introduced as a boundary condition in the hydro-geological model and a new distribution of pore water pressure was obtained for the period in question. Predicted displacements are reported in Figure 10 for borehole B3e at different depths, namely 3 and 9 m. Comparison with the original scenario shows that the drainage system, even if realized at the slope toe, would have a positive effect in terms of movement reduction, including the upper part of the slope.

5 CONCLUSIONS

The geomechanical model proposed to analyse the Steinernase landslide proved its ability in simulating the observed behaviour; in particular, the precision of the model was good enough to reproduce the displacements measured during crisis episodes.
The use of advanced finite element modelling allowed the consideration of specific features of the problem, such as the presence of the multiple slip surface system and the coupling between pore water pressure evolution and movements.

Moreover, the model sheds light on the physical processes involved in the landslide; in particular it appears that the transition from the partially to fully saturated state plays a major role in the accelerations of the superficial material in the landslide.

The analysis of the multiple slip surface mechanism showed that the infrastructure at the toe of the landslide is most directly affected by the deepest slip surface, despite the fact that the movements at the deepest surface were of very low intensities during the measurement campaign. These dangers may be mitigated by drainage at the toe.

PERSPECTIVES

Such an analysis also offers the possibility to include the consideration of dynamic earthquake effects that would be relevant to study, as the region of Basel is one of the most exposed to tremors in Switzerland.

ACKNOWLEDGEMENTS

REFERENCES

Arya, L.M. & Paris, J.F. (1981). A physicoempirical model to predict soil moisture characteristics from particle-size distribution and bulk density data. Soil Sci. Soc. Am. J. 45:1023–1030.

Biot, M.A. (1956). General solution of the equations of elasticity and consolidation for a porous material. Journal of Applied Mechanics, 19:91-96.

EPFL (2008). Geologische, hydrogeologische (GEOLEP) und geomechanische (LMS) Modellierung des Erdrutsches bei Stein-Mumpf (AG). Schlussbericht. Ecole Polytechnique Fédérale de Lausanne, Switzerland.

François, B., Tacher L., Bonnard Ch., Laloui L. and Triguero V. (2007). Numerical modelling of the hydrogeological and geomechanical behaviour of a large slope movement: The Triesenberg landslide (Liechtenstein), Canadian Geotechnical Journal, vol. 44, pp. 840-857, 2007.

Geotest AG (1997). Prüfbericht Labor Nr. Z9608.430.

Geotest AG (2006). Stein-Mumpf Gefahren – und Risikobeur-teliung Vorläufige Ergebnisse. Bericht Nr. Z06015.1/Juni, 2006.

Laloui, L., Klubertanz, G. and Vulliet, L. (2003). Solid-liquid-air coupling in multiphase porous media. International Journal of Numerical and Analytical Methods in Geomechanics, 27(3):183-206.

Nuth M. and Laloui L. (2008). Effective Stress Concept in Unsaturated Soils: Clarification and Validation of a Unified Framework. International Journal of Numerical and Analytical Methods in Geomechanics Vol. 32, pp. 771-801.

Roscoe, K.H. and Burland, J.B. (1968). On the generalized stress–strain behaviour of "wet" clay. In: Engineering plasticity. Edited by J. Heyman and F.A. Leckie. Cambridge University Press, Cambridge, England, pp. 535–609.

Schrefler, B.A. (1984). The finite element method in soil consolidation (with applications to surface subsidence). Doctoral Thesis, University College of Swansea, C/Ph/76/84.

Tacher L., Bonnard Ch., Laloui L. and Parriaux A. (2005). Modelling the behaviour of a large landslide with respect to hydrogeological and geomechanical parameter heterogeneity. Landslides journal, vol. 2, N°1, pp. 3-14, 2005.

Van Genuchten, M.T. (1980). A closed form equation for predicting the hydraulic conductivity of unsaturated soils. Soil Sci. Soc. Am. J. 44:892–898.